ANALYSIS OF THE RATIONALE AND ACCURACY OF THE USE OF CARBON EQUIVALENT AND THERMAL ANALYSIS IN THE QUALITY CONTROL OF CAST IRON

Doru M. Stefanescu
The University of Alabama, Tuscaloosa, AL, USA
The Ohio State University, Columbus, OH, USA

Abstract

The motivation for this paper evolved from the question "when is a cast iron eutectic?" raised by a recent paper. The simple answer is when the carbon equivalent of the iron is 4.2%. This raises another question: How does one calculate the carbon equivalent (CE)? The paper summarizes the many different equations used for this purpose. It demonstrates that Mg and inoculation affect the calculation of CE and that the Si contribution in classic CE equations is inaccurate for all practical purposes. The use of isopleths is limited as they cannot consider the effect of elements such as Mg and oxygen, or that of the metal quality (nucleation potential). They also cannot illustrate the effect of small differences in silicon resulting from inoculation. Corrections for the contribution of Si and Mg are proposed. Yet, CE can be used to determine the eutectic carbon if enough data are available to find the intersection of the austenite and graphite liquidus. Despite its limitations, because of its repeatability for a given process, the foundry can rely on TA and CE for composition control.

Keywords: thermal analysis, carbon equivalent, cast iron, quality control

Background

The scope of this paper is not to cover the vast subject of the use of thermal analysis (TA) as a control tool in the metallurgy of cast iron (we have done that in a previous paper),[1] but rather to discuss the underlining principles and limitations of the use of the concept of "carbon equivalent" by the metal casting industry for quality control of lamellar (LG), compacted (CG) and spheroidal graphite (SG) irons. The carbon equivalent (CE) is a calculated quantity that is used to transfer information on a multicomponent Fe-C-Si-X system on the binary equilibrium Fe-C phase diagram. Assuming that the stable invariant eutectic point in the binary Fe-C system is at $CE = 4.26\%C$,[2] if $CE < 4.26\%$, the iron is hypoeutectic and if $CE > 4.26\%$, the iron is hypereutectic. A simple answer! Or is it? We note that while Okamoto[2] and Neumann[3] use $CE = 4.26\%$, thermodynamic software such as Thermo-Calc (TCFE database) and JMatPro use a value of 4.34%. In addition, it is

important to note that industrial TA has limitations related to uncontrolled cooling condition and transient solidification mode with thermal gradient in the probe that limits the correct evaluation of the eutectic solidification mode in SGI using industrial thermal analysis. Further complications arise in industrial casting, or even the TA cup, as the solidifying alloy may include local mixture of primary graphite and primary austenite precipitated simultaneously.

Before discussing the complexities of the correlation between melt composition and thermal analysis temperature events, it is necessary to have a clear understanding of the solidification sequence of Fe-C-Si-based alloys of hypo- and hyper-eutectic composition in the light of early and latest research findings.

Elements of Solidification of Cast Iron Relevant to the Subject

Early extensive work by Chaudhari et al.[4] established that hypoeutectic LG and SG irons exhibit three characteristic temperatures on the cooling curve: the austenite liquidus

arrest (T_{LA}), the eutectic undercooling, T_{EU} (T_{Emin} in this work), which they considered to be the beginning of the bulk eutectic growth, and the eutectic recalescence, T_{ER} (T_{Emax} in this work). The hypereutectic irons may show up to four characteristic temperatures: the graphite liquidus (T_{LG}), the initial nucleation of the eutectic (T_{EN}), T_{EU} and T_{ER}. This nomenclature is presented schematically in Figure 1 and will be used in the rest of the paper. As shown in Figure 2, mildly hyper-eutectic irons exhibit a T_{EN} and then a flat eutectic arrest (T_{Eut}) with no undercooling and recalescence. Strongly hypereutectic irons show a T_{LG} in addition of the T_{EN}. There is no T_{EN} for hypoeutectic irons.

From this early work, we learn that hypoeutectic SG iron behaves "normally", in the sense that the only phase in the pre-eutectic liquid is austenite. The situation is more complicated for eutectic and hypereutectic SG iron, as this iron solidifies with a divorced eutectic. The cooling curves in Figure 2 suggest that before the eutectic reaction the only phase in the liquid is graphite (T_{LG}).

Recent work with a synchrotron radiation X-ray source by Yamane et al. [5] on hypereutectic irons with 0.02 and 0.05% Mg, found that for both irons, solidification started with graphite particles. For the 0.002% Mg iron, primary dendrite arms appeared at the beginning of the eutectic reaction. As soon as contact was achieved between the austenite dendrites and the graphite, the graphite particles were surrounded by austenite. As the austenite nucleated in the vicinity of the graphite, it appears that the graphite particles were nucleation sites for the austenite dendrites. All the nucleation events occurred within 3 K from the eutectic temperature. For the 0.05% Mg iron, nucleation of graphite particles and austenite dendrites occurred nearly at the same time and they grew independently. Nucleation events of the primary graphite particles continuously occurred until the beginning of eutectic solidification. The temperature range in which the graphite particles grew independently before being engulfed by the eutectic front was only 3 to 4 K. The nucleation frequency of graphite particles in the 0.05% Mg iron was approximately three times larger than that in the 0.002% Mg iron. Also, the high addition of 0.05% Mg slightly decreased the eutectic temperature (6 K) and largely decreased the liquidus temperature (45 K). The Mg addition largely reduced the difference between the liquidus and the eutectic temperatures, from 56 K for 0.002% Mg to 17 K for 0.05% Mg.

Using the direct-austempering-after-solidification technique on irons with 4.24 to 4.59% *CE* (calculated with Eqn. 3) and 0.02 to 0.053% Mg, Boeri et al. [6] concluded that primary graphite and primary austenite precipitated simultaneously in all irons. The nucleation and growth of the austenite dendrites and graphite proceeded independently in the melt. Initially, the graphite particles grow independently in the melt but, as the growing austenite dendrites get in contact with the graphite, graphite-austenite aggregates are formed that grow as cooperative (for LG iron) or divorced (for SG iron) eutectic.

To summarize these experimental findings, it is convenient to incorporate them in previously described mechanisms[7–9]. As summarized in the cellular automaton simulation in Figure 3, primary graphite and primary austenite coexist in the SG iron liquid immediately before the eutectic reaction starts. This means that even in hypereutectic irons austenite dendrites may exist in the liquid. This mode of solidification precludes establishing whether an SG iron is hypo- or hyper-eutectic solely based on metallographic examination and complicates interpretation of the liquidus lines.

The Concept of Carbon Equivalent

Returning to the issue of carbon equivalent, a recent paper by Regordosa et al. [10] raised the question: "when is a cast iron eutectic?" A subsequent analysis by Lekakh[11] argued that a methodology derived solely on industrial TA cannot answer the question without the additional use of direct observation methods. In particular, Lekakh took issue with the fact that the liquidus arrest on the cooling curves of inoculated SG iron solidified in sand cups was identified as a primary graphite liquidus, while the thermal arrest on the non-inoculated SG iron was designated as a primary austenite liquidus. He further questioned Regordosa's conclusion that inoculation triggered switching from hypoeutectic to hyper-eutectic solidification of the iron.
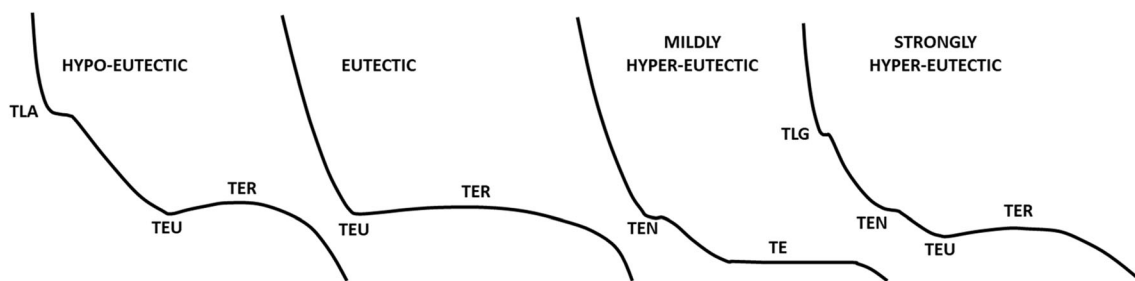

Figure 1. Nomenclature of characteristic temperatures on the cooling curves of SG irons; adapted after Ref. 4.
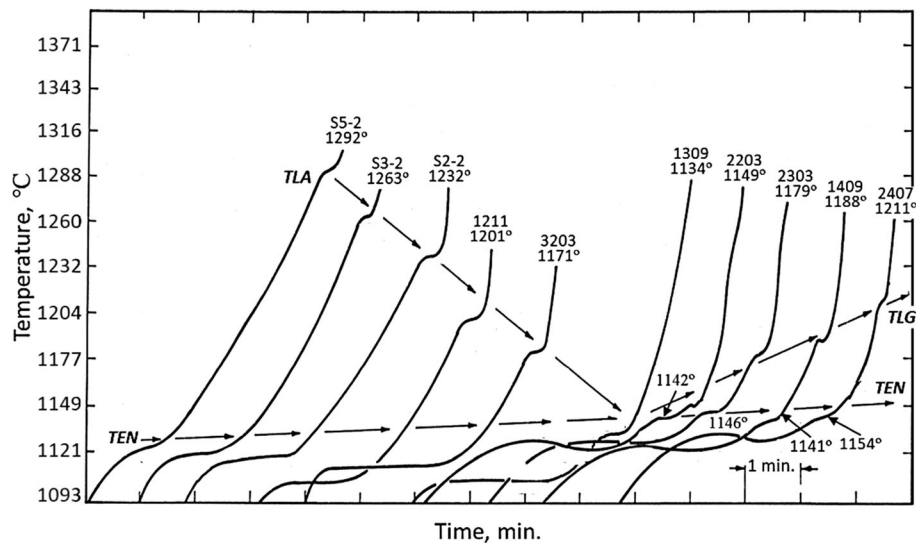
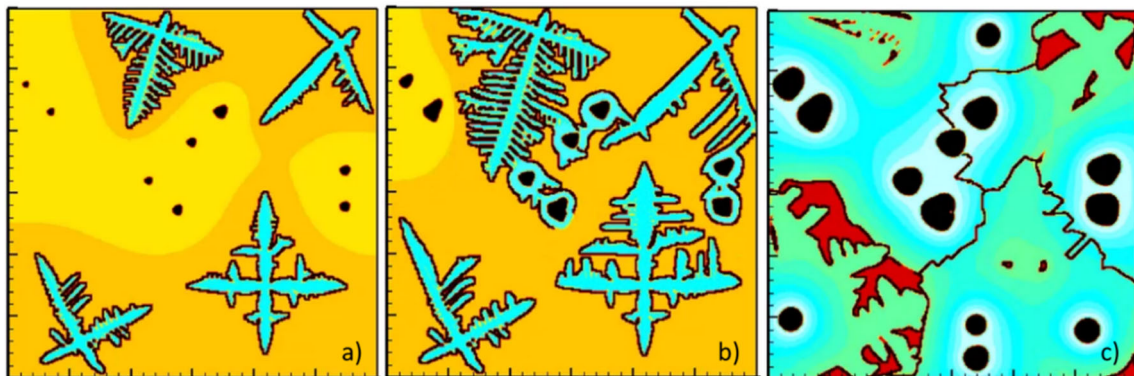**Figure 2. Cooling curves of Ni-Mg-treated cast irons [4].**

Figure 3. Simulation results for the solidification of a continuously cooled SG iron with 3.993 %C [9]: (a) primary austenite and graphite nodules in the liquid; (b) beginning of the divorced eutectic reaction; (c) eutectic grains and residual intergranular liquid immediately before the end of solidification.

So then, can TA alone identify the eutectic invariant for a multicomponent Fe-C-Si alloy? This is the question that we would strive to answer in this paper.

The efforts to correlate the combined effect of C and Si to the microstructure of cast iron (hypo- or hyper-eutectic) go back in time to the nineteenth century. As early as 1892, Ledebur [12] (quoted by Piwowarsky [13]) suggested the equation:

$$CE = (\%C + \%Si)/1.5 \qquad \text{Eqn. 1}$$

In 1933, Schwarz and Vath [14] (quoted by Piwowarsky [13]) built a structural diagram in which they attempted to correlate the microstructure of LG iron with its carbon equivalent employing the equation:

$$CE = \frac{4}{3} \cdot \%Si \cdot \left(1 - \frac{5}{3 \cdot \%C + \%Si}\right) \qquad \text{Eqn. 2}$$

By the 1960s, the metal casting industry used extensively an empirical equation (e.g., Ref [15]):

$$CE = \%C + (\%Si + \%P)/3 \qquad \text{Eqn. 3}$$

Since cast iron is a multicomponent alloy, all the preceding equations are deficient, as they fail to account for the effect of elements such as Mn, S, Mg or O, which are present in cast iron to a greater or lesser extent. Indeed, in 1973, Basutkar et al. [16] showed that the cooling curve method of determining the *CE* of cast iron fails to give a meaningful estimate when the melt is treated with magnesium or cerium. While several equations for *CE* have been developed over the years, acceptance by the industry requires a critical analysis, as some equations may be less scientifically valid, or even erroneous.

Thermal analysis (TA) is used as a control tool to determine the carbon equivalent in industrial practice and thus monitor the chemical composition of the iron. The basic

assumption is that there is a direct correlation between the T_{LA} and CE. There are several problems with the method. The solidification of iron is a non-equilibrium process, which complicates the attempt to relate to the equilibrium phase diagram, as the experimental cooling curve will exhibit undercooling with respect to the equilibrium temperatures. The cooling rate, the mass of the casting and metallurgical factors such as furnace-holding before treatment with Mg (remember "Monday morning melt"), inoculation and holding after inoculation will determine the extent of deviation of the experimental T_{LA}^{exp} from the equilibrium T_{LA}^{eq}.

The accuracy, reproducibility, and sensitivity of the T_{LA}^{exp} recorded by the TA system are a function of the equipment quality and of the measuring and process parameters. The equipment characteristics of interest include: the geometry and the material of the cups; the performance of the measurement technology, including electrical accuracy of the time/temperature signal, the smoothing of the measured values, and the calibration and sensitivity of the thermocouple (TC) [17]. The most important measuring parameters are the mass of iron in the cup and the pouring temperature (registered as the maximum temperature of the cooling curve). They directly affect the solidification kinetics as they change the cooling rate. The processing parameters include what in metal casting lingo is known as the "metal quality", some metallurgical characteristics difficult to know prior to casting, such as the nucleation potential, the degree of oxidation of the melt, and the chemistry of the melt to include not only the base elements (C, Si, Mn, P, S), but also the alloying and trace elements. These challenges are the object of the following sections.

Measuring Methods

In the metal casting industry, TA is conducted by inserting a thermocouple in selected positions in the mold or by means of special standardized measuring devices. One or more cooling curves are recorded, and then, computer analysis of the digital data is used to extract information relevant to the composition and solidification of the iron. Commercial devices designed for process control in metal casting include thermal analysis cups and analyzing software. The most common TA devices use sand cups of various designs with one (1TC) or two (2TC) thermocouples inserted in the cup. The Electro-Nite 1TC sand cup is presented in Figure 4a. For the Electro-Nite cup, the mass of iron in the cup can be controlled by slight overpouring. However, in practice operators may underfill the cup.

There are several other notable commercial systems that use the Electro-Nite sand cup, including Thermolan and MeltLab®. The MeltLab® system is known particularly for the use of higher derivatives (up to the 5th derivative) [18] made possible by a proprietary signal processing software, which reduces or eliminates the noise of the recorded data.

A second design is the 2TC Kuehn AccuVo® dual sand cup, [19] presented in (Figure 4b). This system has the advantage of controlling the mass of iron in the cup by the very design of the AccuVo® cup, which includes two spherical test cavities with risers. The two spherical cavities can be used either for the direct comparison of uninoculated (TC in the middle of cavity 1) and inoculated irons (TC in the middle of cavity 2), or with one TC in the middle of cavity 1, and a second TC close to the wall cavity 2 (Figure 4c) to obtain information on the development of the dendritic structure as in ref. [20]. For all sand cups, the pouring temperature can be controlled by an additional thermocouple in the pouring ladle.

A completely different design is the 2TC SinterCast immersion steel cup [21] shown in Figure 4d. It is a further development of the steel cup with immersion holes developed by Ryntz et al. [22] and by Bäckerud et al. [23]. The SinterCast metal cup is fully immersed in the molten iron and is removed at the set temperature indicated by the thermocouple in the cup. Its design controls both mass and temperature. The cup and the metal cool in equilibrium. By contrast, the heat capacity of the sand cups extracts heat from the metal; the temperature of the iron influences the heating of the sand, and the sand influences the cooling of the iron.

The design differences of the cup (pour-in sand or immersion metal) will produce differences in the recoded cooling curves as shown in Figure 5. The TA curves in Figure 5a were from 8 tons melts where Mg treatment and inoculation were added. SG iron shows the highest undercooling. The TA curves in Figure 5b were obtained from melts produced in a 22.7 kg induction furnace, treated with Mg-FeSi and then returned to the furnace. The furnace was set on hold, and TA curves samples were poured sequentially every two or three minutes [24]. The CG iron shows the highest undercooling.

The effect of equipment quality on the accuracy of the recorded cooling curve was extensively discussed by Kuehn [17]. The example in Figure 6a presents a comparison between the cooling curves of a hypo-eutectic cast iron obtained with a standard low-frequency device (black line) and with the optimized 20–40 Hz high-frequency device (gold line) [25]. The definitions of the solidification events are as suggested by Kuehn. It is seen that because of the improved silica protection tube thickness and thermocouple diameter, the optimized sensor (gold) can resolve the liquidus recalescence (T_{LA}^{opt} vs. T_{LA}^{st}). In addition, the weak exothermic event next to the end of solidification exhibits clear recalescence for the optimized curve (T_{end}^{opt}), while it shows only a slight inflection for the standard one (T_{end}^{st}). Weak inflections are seen about 20 °C above the liquidus
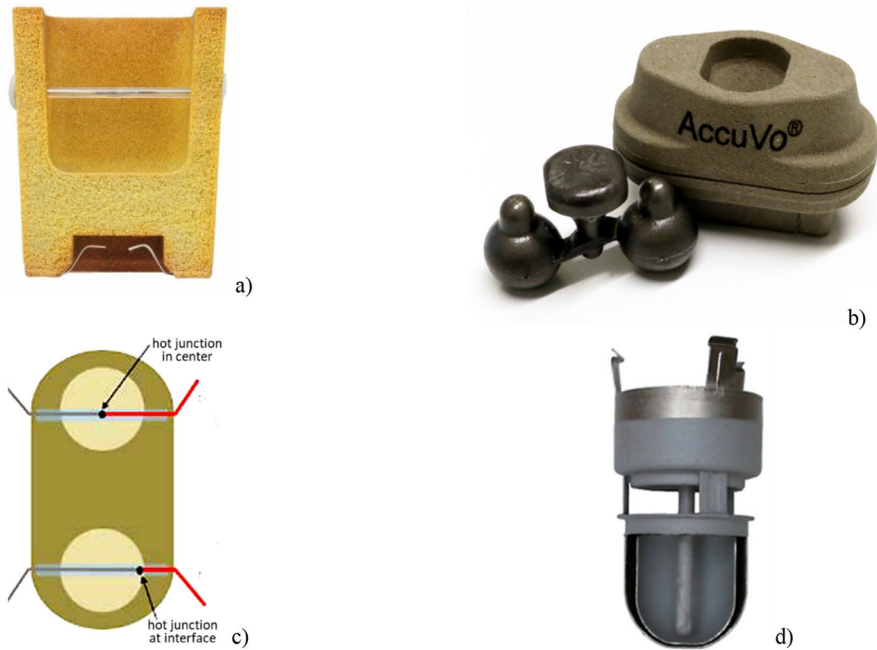
Figure 4. Examples of test cups for cooling curve analysis; (a) sand cup (QuiK-Cup) with disposable thermocouple (Electro-Nite); (b) closed double chamber crucible AccuVo® [19]; (c) AccuVo® cup with center and side thermocouple [20]; (d) steel cup (SinterCast) with two thermocouples in the protective central tube [21].
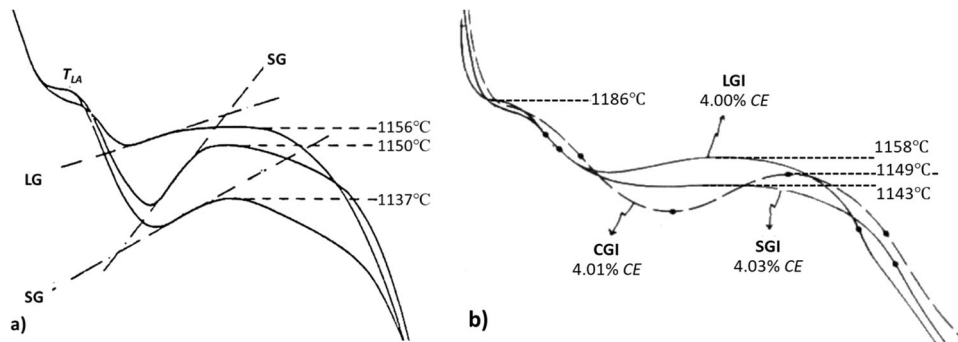

Figure 5. Effect of TA cup design on the recorded cooling curves: (a)1TC immersion steel cups [23]; (b) 1TC sand cups [24].

(T_{preLA}^{opt} vs. T_{preLA}^{st}). According to Sparkman, quoted by Kuehn, they reflect a possible reaction of iron and silicon in the presence of oxygen.

The explanation of these differences is illustrated in Figure 6a, where the data of standard and optimized thermocouple are compared. The cooling curves displayed by the TA equipment are the result of the thermocouple setup that expresses itself in a distinct difference in sensor sensitivity and precision.

As there is a direct correlation between the quality of the smoothing and the sampling rate, a high frequency (higher sampling rate) will generate a precise image of the analog signal that is illustrated in inset (b). Thus, the optimized

filtered curve follows exactly the raw data taken with a frequency of 40 points per second from the TSK A/D converter, while the standard one produces a continuous line without a thermal event. The figure also compares the exothermic event next to the end of solidification (see inset (a)) for data acquired with a standard (large circles, black line), with data generated by an optimized A/D converter from TSK (gold).

Methods Used in the Generation of Carbon Equivalent Equations

Over the years, several approaches have been used to define the *CE*, including regression analysis of
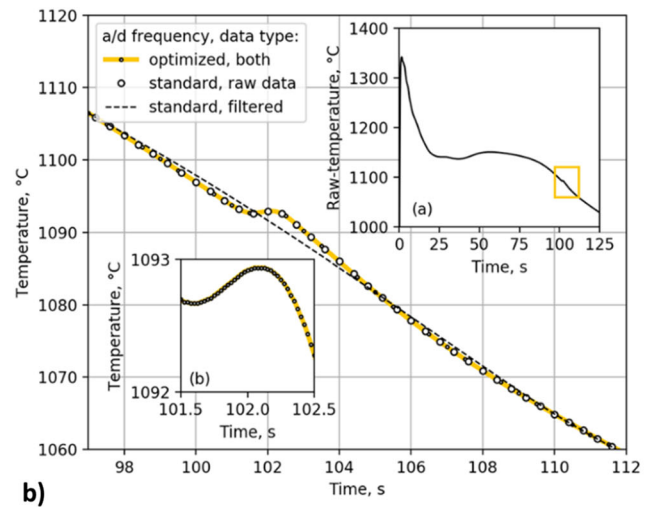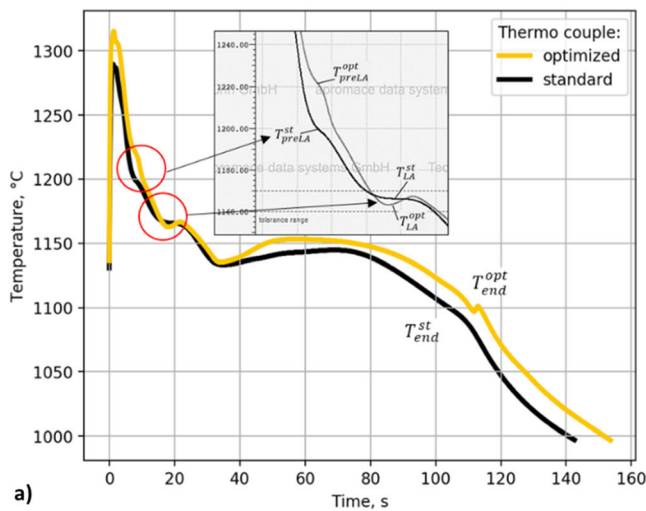
Figure 6. *Effect of equipment quality: (a) cooling curves from a closed double chamber crucible AccuVo® equipped with an optimized (gold) and a standard thermocouple (black); (b) comparison between the raw data from the A/D with converter and the filtered temperature data provided by a standard A/D, on the one hand, and the optimized A/D converter by TSK, on the other hand [25].*

experimental data (empirical approach), thermodynamic calculation, calculations using the linearized slopes of the liquidus lines of the binary Fe-C diagram, and regression analysis of data generated from polythermal cross sections of multicomponent Fe-C diagrams obtained with the Thermo-Calc software. It is important to note that this is an equilibrium CE_{Eq} that does not include the effects of processing parameters of the industrial cast iron.

The Empirical Approach

As early as 1961, Humphreys [26] generated a regression equation correlating the carbon equivalent with the liquidus temperature of industrial cast iron measured with a standard thermal analysis cup. Thus, Humphreys recognized that the measured T_{LA} is lower than the thermodynamic equilibrium liquidus temperature and is only valid for the type of cup that he used. Consequently, this carbon equivalent was dubbed Carbon Equivalent Liquidus, *CEL*. Its equation and the correlation with the liquidus temperature were given as:

$$CEL = \%C + 0.25 \cdot \%Si + 0.5 \cdot \%P$$
$$CEL = 13.46 - 0.0081 \cdot T_{LA} \qquad \text{Eqn. 4}$$

where *%C, %Si* and *%P* are the amounts of elements (mass percent) in the melt found through chemical analysis.

Heine [27] established several empirical relationships between the characteristic temperatures and the composition of cast irons, as follows:

$$T_{LA} = 1582.4 - 97.3 \cdot CEL \; where \; CEL$$
$$= \%C + 1/3 \cdot \%Si \qquad \text{Eqn. 5}$$

$$T_{LA} = 1569 - 97.3 \cdot CEL \; where \; CEL = \%C + 0.25 \cdot \%Si$$
$$\text{Eqn. 6}$$

$$T_{LG} = 389.1 \cdot CEL - 505.8 \; where \; CEL$$
$$= \%C + 1/3 \cdot \%Si \qquad \text{Eqn. 7}$$

The eutectic carbon was calculated to be:

$$C_{Eut} = 4.26 - 0.317 \cdot \%Si \qquad \text{Eqn. 8}$$

Sillén [28] argued that as carbon equivalent is affected by the cooling rate and the nucleation level, the active carbon equivalent (*ACEL*) should be used:

$$ACEL = 14.45 - 0.0089 \cdot T_{LA} \qquad \text{Eqn. 9}$$

All these equations describe a carbon equivalent that includes processing parameters other than the simplified chemical analysis, including a defined cooling rate specific to the sand cup used, as well as the specific pouring temperature and the metallurgical particularities (melt degree of oxidation, inoculation, holding times). Thus, it should be called kinetic carbon equivalent, CE_{Kin}. This is different from the equilibrium carbon equivalent, CE_{Eq}, which is calculated based on thermodynamics and phase equilibria, as discussed in the following sections and is only a function of composition.

The Thermodynamic Approach

In 1968, Neumann [3] produced the first attempt at thermodynamic calculations, postulating that the changes in carbon solubility in the liquid metal resulting from additions

of third elements, X, can be calculated with the relationship:

$$\Delta\%C_{liq}^{X} = m_X \cdot \%X \qquad \text{Eqn. 10}$$

where m is the solubility factor, and $\%X$ is the amount of third element. The solubility factors of various third elements for carbon-saturated ternary Fe-C-X melts were measured and calculated through thermodynamics principles, as summarized in Table 1. It was noted that "*several researchers have established that the solubility factors are only slightly dependent on temperature*" [3]. The eutectic carbon was then calculated as:

$$\begin{aligned} C_{Eut} &= 4.26 + \Delta\%C^{Si} + \Delta\%C^{Mn} + \Delta\%C^{P} + \Delta\%C^{S} + \dots \\ &= 4.26 - 0.31 \cdot \%Si - 0.33 \cdot \%P - 0.4 \cdot \%S + 0.027 \\ &\quad \cdot \%Mn + \dots \end{aligned}$$
$$\text{Eqn. 11}$$

Then, assuming that the carbon equivalent for the multicomponent solution has the same carbon activity as the equivalent amount of carbon in the binary solution, an equilibrium carbon equivalent, CE_{Eq}, is calculated as the carbon content in the melt, $\%C$, plus the amount of carbon equivalent from the added elements, $\sum \Delta C^X$, as:

$$\begin{aligned} CE_{Eq} &= \%C - \Delta\%C^{Si} - \Delta\%C^{Mn} - \Delta\%C^{P} - \Delta\%C^{S} - \dots \\ &= \%C - \sum \Delta C^X \end{aligned}$$
$$\text{Eqn. 12}$$

Introducing the experimental values, m_X^{exp}, of the solubility factors of various third elements for carbon-saturated Fe-C-X melts (column 2 in Table 1) in this equation, Eqn. 13 in Table 2 is obtained. Equation 13 is the equation of choice for the carbon equivalent of cast iron in the ASM Handbook 2017 edition [29]. For comparison, the CE_{Eq} equation generated when the theoretical Neumann solubility factors are used is given in Table 2 as Eqn. 14.

Using a different derivation than that of Neumann, thermodynamic calculations by Creese and Healy [30] for a 3.5%C iron utilizing available interaction coefficients for a liquid iron temperature of 1500 °C produced slightly different solubility factors (Table 1) and a less complete equation (Eqn. 15 in Table 2). We note that while the calculated value for m_{Si} by Neumann is -0.28, that proposed by Creese and Healy is -0.32, which is closer to the experimental values obtained by Neumann (-0.31) and by Heine [31] (-0.317).

It is important to note that the thermodynamic CE_{Eq} equation is developed on the assumption that the solubility factor m_X is independent of temperature and of the amount of element X.

The Thermo-Calc Approach

Calculations of the solubility factors have also been made for Fe-C-Si-X alloys with 2.5 mass% Si at the stable eutectic composition and temperature with the Thermo-Calc TCFE8 software [29]. The results are very close to the experimental values by Neumann listed in Table 1. The corresponding CE_{Eq} equation is Eqn. 16 in Table 2.

Table 1. Experimental (exp) and Calculated (calc) Solubility Factors of Various Third Elements for Carbon-Saturated Fe-C-X Melts in the Stable System.

Element	Neumann Ref. 3		Creese Ref. 30	Thermo-Calc Ref. 29	Bazhenov Ref. 32	Castro Ref. 33
	m_X^{exp}	m_X^{calc}	m_X^{calc}	m_X^{calc}	m_X^{calc}	m_X^{calc}
Al	−0.220	−0.215	–	−0.031	–	–
Si	−0.310	−0.294	−0.32	−0.280	−0.30	−0.280
P	−0.331	−0.349	−0.33	−0.299	−0.33	−0.303
S	−0.405	−0.414	–	−0.170	−0.26	–
Ti	+0.159	+0.138	–	+0.162	–	–
V	+0.105	+0.097	–	+0.094	–	–
Cr	+0.064	+0.062	–	+0.078	–	−0.033
Mn	+0.028	+0.029	–	+0.010	+0.015	−0.007
Co	−0.027	−0.029	–	−0.033	–	–
Ni	−0.051	−0.055	–	−0.043	–	−0.054
Cu	−0.076	−0.080	–	−0.051	–	−0.092
Mo	+0.014	−0.012	–	+0.001	–	−0.011
W	−0.015	−0.010	–	−0.026	–	–

Table 2. Carbon Equivalent Equations for Multicomponent Fe-C-Si Alloys.

Eqn.	Carbon equivalent, CE_{Eq}	Ref	*
Eqn. 13	$\%C + 0.31 \cdot \%Si + 0.33 \cdot \%P + 0.41 \cdot \%S - 0.027 \cdot \%Mn - 0.064 \cdot \%Cr + 0.076 \cdot \%Cu.$	3	E
Eqn. 14	$\%C + 0.29 \cdot \%Si + 0.35 \cdot \%P + 0.41 \cdot \%S - 0.029 \cdot \%Mn - 0.062 \cdot \%Cr + 0.080 \cdot \%Cu$	3	TD
Eqn. 15	$\%C + 0.32 \cdot \%Si + 0.33 \cdot \%P$	30	TD
Eqn. 16	$\%C + 0.28 \cdot \%Si + 0.30 \cdot \%P + 0.17 \cdot \%S - 0.010 \cdot \%Mn - 0.033 \cdot \%Cr + 0.051 \cdot \%Cu.$	29	TC
Eqn. 17	$\%C + 0. \cdot \%Si + 0.33 \cdot \%P + 0.26 \cdot \%S - 0.015 \cdot \%Mn.$	32	TC
Eqn. 18	$\%C + 0.28 \cdot i + 0.30 \cdot \%P + 0.007 \cdot \%Mn + 0.092 \cdot \%Cu$	33	SL

*: *E* experimental; *TD* thermodynamic calculation; *TC* Thermo-Calc based; *SL* slopes of liquidus lines

In a recent paper, Bazhenov and Pikunov [32] determined the carbon equivalent by means of polythermal cross sections of the Fe–C–Si–P–Mn–S system plotted using the Thermo-Calc program. A total of 81 polythermal cross sections of the Fe–C–Si–P–Mn–S system for carbon were calculated with three levels of Si, P, Mn, and S. Regression analysis was then used to evaluate the carbon equivalent. The calculated solubility factors are given in Table 1, and the corresponding equation is presented in Table 2 as Eqn. 17. It is seen that the solubility factors for Si and P are very close to the experimental ones by Neumann, but those for S and Mn are about half of the experimental ones.

The Estimation of the Slope of the Liquidus Line Approach

Castro et al. [33], working on the assumption that the liquidus temperatures of austenite and graphite can be expressed by linear relations to composition, and then estimating the slopes of these lines from phase diagram information, calculated solubility factors in the range of other calculations for Si, P, Ni and Cu. However, for Mn and Cr, their values have a negative sign, in contradiction with all other calculated or experimentally measured data (see Table 1). The corresponding equation is given in Table 2 as Eqn. 18. It is seen that the solubility factors for Si and P are lower than the experimental ones by Neumann or Heine and the effect of S is not considered. In addition, this is the only calculation that produces a positive sign for Mn, a carbide promoter. This runs contrary to the accepted theory that a positive solubility factor indicates a low graphitization potential, i.e., a carbide forming tendency.

Effect of Magnesium

Basutkar et al. [16] studied irons with chemical composition in the range 3.22–3.86% C, 1.62–2.68% Si. 0.04–0.06% Mg, and two levels of cerium, 0.02 and 0.03% Ce. Cooling curves were obtained from cylindrical sand test castings 12.7 cm in diam. and 30.5 cm high cast against chills. They concluded that solidification temperatures in heavy sections approach equilibrium temperatures, that rapid cooling causes the arrest corresponding to the temperature of graphite liquidus to disappear although the growth process associated with it still occurs. Based on the displacement of the *CE* in irons modified with Mg and Ce compared with the non-treated irons, they suggested that the *CE* equation for Mg- and Ce-treated irons should include additional coefficients, as follows:

$$CE = \%C + 0.25 \cdot \%Si - 0.7 \cdot \%Mg - 1.25 \cdot \%Ce$$

$$\text{Eqn. 19}$$

Recent work by Yamane et al. [5] on hypereutectic SG iron (3.73% C, 2.57% Si, 0.45% Mn, 0.004% S, 0.05% Mg) using a synchrotron radiation X-ray source suggests that the temperature difference between the liquidus and the eutectic temperatures decreased with the addition of Mg explained by the shift of the eutectic composition to the carbon side as Mg concentration increases (Figure 7). As the eutectic composition shifts to the carbon side with increased Mg, the influence of Mg addition can be consistently explained. Consequently, a new empirical carbon equivalent was defined as:

$$CE = \%C + \frac{1}{3} \cdot \%Si - 6 \cdot \%Mg \qquad \text{Eqn. 20}$$

The Mg solubility factor $m_{Mg} = -6$ suggested by Yamane et al. is an order of magnitude higher than the -0.7 suggested by Basutkar et al.

Based on this, on the previous analysis of various models, and on the analysis of experimental data, the following Neumann-based equation will be used in further analysis when assuming $C_{Eut} = 4.26$:

$$\begin{aligned} CE_{Eq} = &\%C + 0.31 \cdot \%Si + 0.33\% \cdot P + 0.31 \cdot \%S \\ &- 0.02\% \cdot Mn - 0.062\% \cdot Cr + 0.076\% \cdot Cu \\ &- m_{Mg} \cdot \%Mg \end{aligned}$$

$$\text{Eqn. 21}$$

The contribution of magnesium is included through the solubility factor, m_{Mg}, which based on previous research can take values between -0.7 and -6.

Research Strategy

A large number of experimental data were compiled and included in Appendix. The main experimental details for these data are summarized in Table 3. Table 5 includes data from Chaudhari et al. [4] obtained with 1TC sand cups. Table 6 is a selection of data from the work of Alonso et al. [34] where two thermocouples were placed in specially designed mold, one close to the upper surface and the other close to the bottom (see Figure 3 in the ref. for details). The difference in position affected the cooling rate, as the bottom thermocouples registered faster solidification rates. Anjos [35] performed TA measurements with AccuVo® double chamber closed cups with a thermocouple in each chamber that allows direct comparison between inoculated and non-inoculated Mg-treated melts (Table 7). Tables 8 and 9 include the data published by Regordosa et al. [10, 36]. The data were generated with the Thermolan system (1TC sand cup) from an iron treated with Mg-FeSi held in an 8 tons pressurized pouring unit. Two TA cups were poured from the unit at increasing holding time intervals. One of the TA cups was empty, while the other one had some commercial inoculant on the bottom. Table 10 includes data from the work of Ai et al. [37] that studied the effect of inoculation on the liquidus temperature of CG irons produced through Mg-wire (Mg8.5-45Si-4.5RE) treatment and Fe-Si55-Ca2-Ba6 wire inoculation).

All these data were generated with the use of sand as a material for the containment of the molten metal. Courtesy of Dawson and Popelar [38] data obtained with metal cups are also included in this study in Table 11. More details on the process will be provided later in this paper.

All these data were used to calculate the carbon equivalent with various equations and to estimate the effect of inoculation. Data analysis was performed by producing CE - T_L diagrams and comparing them with the equilibrium binary Fe-C diagram calculated with Eqn. 21 and, when possible, also with Fe-C-Si isopleths for various silicon contents.
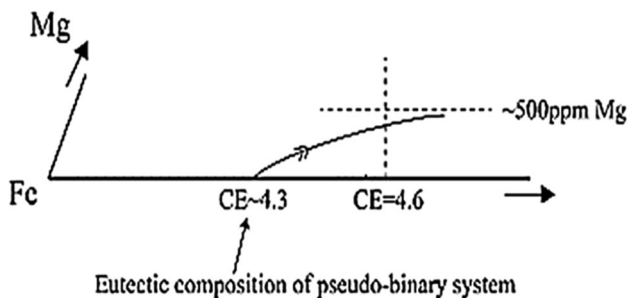

Figure 7. Schematic illustration of isothermal section in Fe-C-Mg pseudo-ternary system around the Fe-C eutectic composition [5].

Results and Discussion

As previously stated, early carbon equivalent equations only included the effect of Si and P. However, cast iron is a multicomponent alloy. Its composition includes base elements (C, Si, Mn, P, S), alloying elements (Cu, Ni, Cr, etc.) and trace elements that include gasses such as nitrogen and oxygen. All of these affect the carbon equivalent. Of particular interest is the effect of Mg as this element is present in both spheroidal and compacted graphite irons. In addition, the melting conditions that include superheating and holding of the iron in the furnace, inoculation and pouring temperature will also have an influence on the critical temperature registered by the thermocouple. Let us first analyze the accuracy of the current CE equations in predicting the eutectic carbon.

Accuracy of Current CE Equations

The experimental liquidus temperatures of Chaudhary et al. [4] for data with silicon contents between 2.2 and 2.7% (average 2.5%) were superimposed on the equilibrium Fe-C diagram in Figure 8a. The T_{LA} and T_{LG} lines of the binary Fe-C equilibrium diagram were calculated with:

$$\%C = 2.11 + 1.213 \cdot 10^{-3} \cdot T_{LG} + 5.197 \cdot 10^{-7} \cdot T_{LG}^2$$

Eqn. 22

$$\%C = 16.6456 - 107.92 \cdot 10^{-4} \cdot T_{LA}$$

Eqn. 23

Equation 22 is taken from ref. 29. Equation 23 is a linear approximation of the liquidus line in the Fe-C diagram according to Okamoto [2].

As seen in Figure 8a from regression lines calculated with data from Table 5 with Eqn. 21 ($m_{Mg} = 0$) for CE, the austenite liquidus temperature (T_{LA}) of the Chaudhari data is above the liquidus of the equilibrium Fe-C diagram for both LG and SG irons, while the graphite liquidus (T_{LG}) is under the equilibrium one. Both the T_{LA} and T_{LG} are decreased by Mg treatment. The point of intersection of T_{LA} and T_{LG} gives the experimental eutectic composition and temperature. The eutectic CE appears to be 4.5 for LG and 4.49 for SG iron. This is significantly higher than the eutectic carbon $C_{Eut} = 4.26$ of the Fe-C diagram, which makes the irons hypereutectic. The figure shows a decrease in the T_{EUT} of the SG iron with respect to the LG iron, and a slight decrease in the eutectic composition.

The same data plotted on the Fe-C-2.5% Si isopleth are shown in Figure 8b. Now, all T_{LA} and T_{LG} are undercooled with respect to the equilibrium liquidus and the experimental eutectic composition is only slightly hypereutectic, very close to the equilibrium $C_{Eut} = 3.7$. In both Figure 8a and b, it is seen that while the LG iron T_{LG} line is parallel to the equilibrium Fe-C or Fe-C-2.5Si lines, the SG iron

Table 3. Summary of Research Details.

Research team	Abbreviation on graphs	TA method	Material	Mg-treatment	Inoculation
Chaudhari et al. [4]	Chaudh	1TC sand cup	LG, SG	NiMg in ladle	no
Alonso et al. [35]	Alonso	1TC sand mold	SG	Mg-FeSi in ladle	in-mold
Anjos [35]	Anjos	2TC double chamber closed cups	SG	Mg-FeSi in ladle	in cup
Regordosa et al. [37]	Regord1	1TC sand cup	SG fading to LG	Mg-FeSi in ladle, holding in pressure-pour	1st cup no
					2nd cup yes
Regordosa et al. [10]	Regord2	1TC sand cup	SG	Mg-FeSi in ladle	1st cup no
					2nd cup yes
Ai et al. [37]	Ai	1TC sand cup	CG	Mg wire	in cup
Dawson, Popelar [38]	Sinter A,C,H	2TC metal cup	CG	Mg wire	in ladle

T_{LG} line increasingly diverges from the equilibrium line with higher temperatures. As previously discussed, Yamane et al. [5] demonstrated that nucleation of graphite particles and austenite dendrites in hypereutectic irons occurred nearly at the same time and they grew independently, as illustrated in Figure 3. Nucleation events of the primary graphite particles continuously occurred until the eutectic solidification commenced. This means that a local hypereutectic mode, when graphite nodules grow in direct contact with the melt, may coexist with a local hypoeutectic mode, when primary austenite dendrites were formed from the melt. Consequently, the T_{LG} appears to include the combined thermal effects of these two solidification events. This is particularly plausible in inoculated irons where constitutional undercooling occurring in Si-rich areas surrounding the dissolution of the inoculant favors graphite precipitation in an otherwise hypoeutectic melt.

So, the CE calculated with Eqn. 21 significantly overestimates the eutectic carbon, which for irons with 2.5%Si is of 3.7% as shown in Figure 8b. This overestimation is caused by the inaccuracy in the solubility factors resulting from two assumptions: (1) Solubility factors are independent of temperature (they are not); (2) solubility factors are independent of the amount of third element (Si). Note that Neumann [3] restricted the validity of the solubility factor for Si in Table 1 to %Si<5.5.

To check the validity of the second assumption, the correlation between the eutectic carbon and %Si is plotted in Figure 9 for several Fe-C-Si isopleths together with Neumann's Eqn. 11. The various equations obtained using linear and polynomial trend lines are listed in Table 4. It is seen that all the slopes of the isopleths data (m_{Si}) are smaller than the -0.31 obtained experimentally by Neumann. The Neumann line lies significantly under the isopleths data. We note that for the range 0 to 3.9% Si, $m_{Si} = -0.3$, which is the same as that obtained in ref [32] This suggests that the main reason of

the discrepancies in Figure 8 is caused by the values attributed to the effect of Si.

The best fitting for silicon is obtained with the polynomial equation:

$$C_{Eut} = 4.34 - 0.19 \cdot \% \ Si - 0.031 \cdot \% \ Si^2 \qquad \text{Eqn. 24}$$

Based on this analysis, a modified CE equation summarized from Thermo-Calc data in Table 1 and Bazhenov and Pikunov work [32] is offered here to be used when assuming that $C_{Eut} = 4.34$:

$$\begin{aligned} CE_{Eq} = \ & \%C + 0.19 \cdot \%Si + 0.031 \cdot \%Si^2 + 0.33 \cdot \%P \\ & + 0.26 \cdot \%S - 0.015 \cdot \%Mn - 0.033 \cdot \%Cr + 0.05 \\ & \cdot \%Cu - m_{Mg} \cdot \%Mg \end{aligned}$$

$$\text{Eqn. 25}$$

When plotting the Chaudhari et al. [4] data with the use of the modified Eqn. 25 for $m_{Mg} = 0$ (Figure 8c), it is seen that the irons are just slightly hypereutectic, as also indicated by the Fe-C-2.5Si isopleth in Figure 8b. This confirms the validity of Eqn. 25.

It is also worth noting that in work by Pan et al. [39], samples having 3.65% C and 2% Si were considered hypereutectic based on their $CE = 4.3\%$ calculated with Eqn. 3. Yet, the samples show a clear austenite liquidus arrest. When recalculating the carbon equivalent with Eqn. 25, the CE changes to 4.15, which makes the irons hypoeutectic explaining the austenite liquidus arrest. Similarly, in the work of Boeri et al. [6] a CE range of 4.24 to 4.59% is calculated with Eqn. 3, which means that all irons are hypereutectic. When Eqn. 25 is used, the range becomes 4.07 and 4.13%, making the irons hypoeutectic.

Figure 8 also shows that for iron melts prepared under similar conditions and measured with the same equipment,
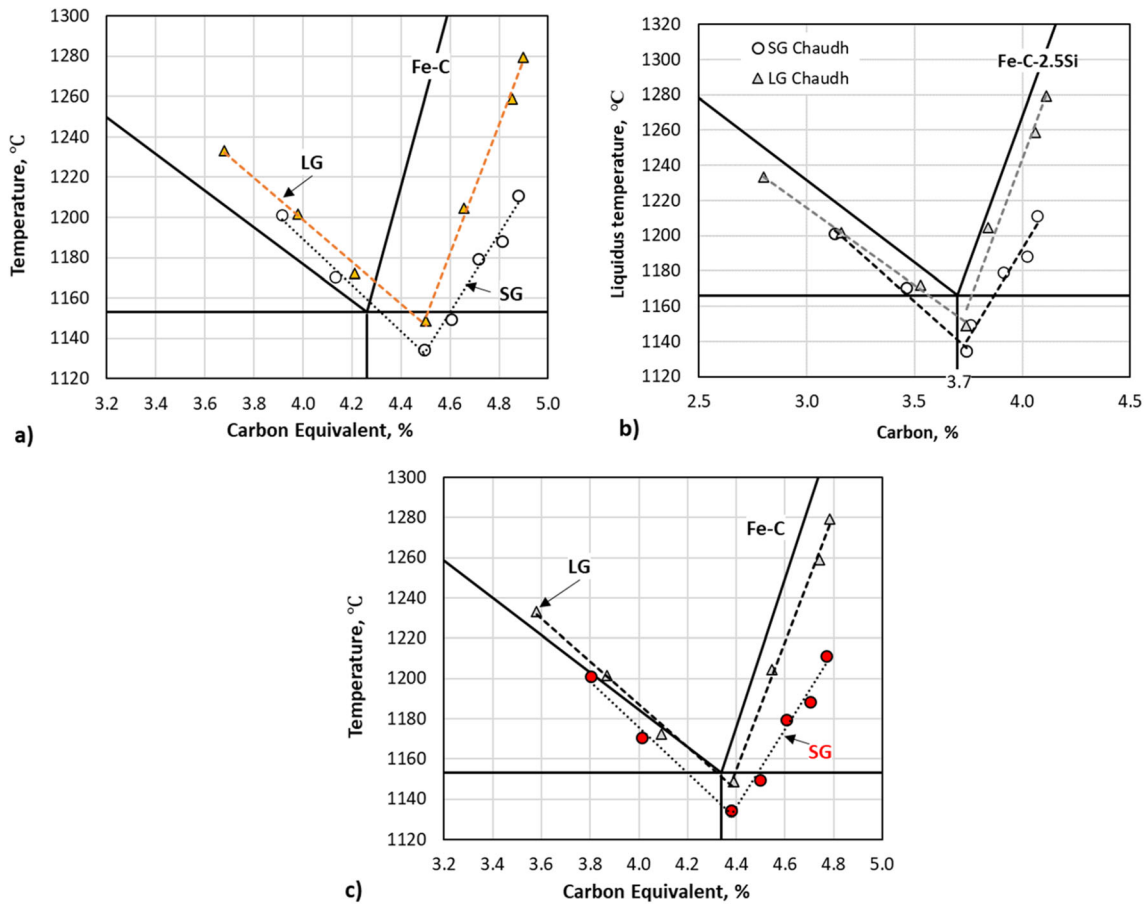
Figure 8. Austenite and graphite liquidus of uninoculated irons; data with about 2.5% Si from ref. 4: (a) as a function of carbon equivalent calculated with the Neumann-based Eqn. 21 superimposed on the Fe-C diagram; (b) as a function of carbon with Eqn. 21 superimposed on the Fe-C-2.5Si isopleth; (c) as a function of carbon equivalent calculated with the Thermo-Calc based on Eqn. 25 superimposed on the Fe-C diagram with $C_{Eut} = 4.34$.

the eutectic composition can be evaluated from TA, if the intersection between the T_{LA} and T_{LG} lines is available.

Effect of Magnesium

Chaudhary et al. [4] discussed the effect of Mg in terms of changes of the significant temperatures on the cooling curves, but not with respect to the carbon equivalent. No equations were derived to quantify the effect of Mg. Yet, the information is available in the data. By extending the T_{LA} line of the LG irons in Figure 8c to the eutectic temperature of the SG iron, it is calculated that the averaged Mg residual of 0.057% has displaced the eutectic carbon to the left by 0.11%, which implies a solubility factor $m_{Mg} = -1.05$. This number appears to slightly decrease with lower undercooling. It is also reasonably close to the -0.7 earlier suggested by Basutkar et al. [16]. When this factor is used in Eqn. 25, the Mg-treated irons become hypoeutectic (Figure 10).

T_{LA} and T_{LG} data for SG irons from various investigators are compared in Figure 11. The carbon equivalent was
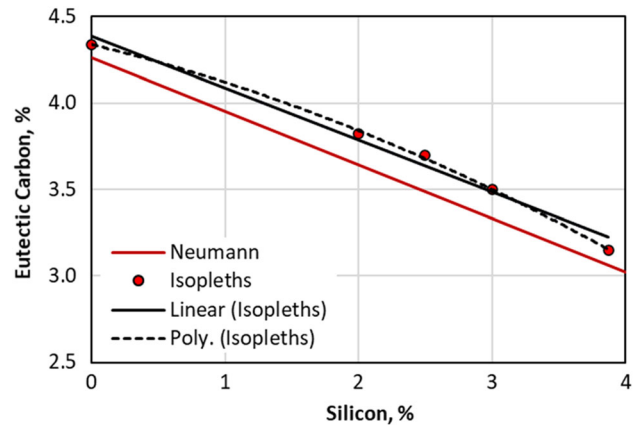

Figure 9. Correlation between the silicon content and eutectic carbon for Fe-C-X% Si isopleths.

calculated with Eqn. 25 ignoring the effect of Mg ($m_{Mg} = 0$) in Figure 11a, and with the same equation but including the effect of Mg ($m_{Mg}^{exp} = -1.05$) in Figure 11b. The Chaudhari trend lines previously shown in Figure 10 are also included in the figure. When the Mg contribution is

Table 4. Correlations Between Eutectic Carbon (C_{Eut}) and Percent Silicon from Fe-C-Si isopleths.

%Si range	Trend line	Equation for C_{Eut}	m_{Si}
0–2	linear	$4.34 - 0.260 \cdot \%Si$	−0.260
0–2.5	linear	$4.34 - 0.257 \cdot \%Si$	−0.257
0–3.0	linear	$4.35 - 0.257 \cdot \%Si$	−0.257
0–3.9	linear	$4.38 - 0.300 \cdot \%Si$	−0.300
0–3.9	polynomial	$4.34 - 0.19 \cdot \%Si - 0.031 \cdot \%Si^2$	–

ignored, good agreement is seen for the Chaudhari data (1TC standard TA sand cup, no inoculation), the Alonso data (in-mold inoculation and various cooling rates) and Anjos data (AccuVo® dual sand cup, inoculation), even though there are significant differences in the silicon content and cooling rate (Figure 11a). The convergence of the T_{LA} and T_{LG} fitting lines suggests roughly a eutectic composition of 4.38% CE_{Eq}. However, the Regordosa1 data (1TC standard TA sand cup, no inoculation) are shifted to the right on a line parallel to the T_{LA} of the other data.

Calculation of the CE with $m_{Mg}^{exp} = -1.05$ to include the effect of magnesium, presented in Figure 11b, shows remarkable differences. Magnesium displaces the liquidus lines and the eutectic composition to the left. The convergence of the T_{LA} and T_{LG} lines suggests a stable eutectic invariant of 4.32% CE_{Eq} for the Chaudhary uninoculated irons.

An excellent data base for the purpose of this analysis was provided by Regordosa et al. [36] (see Table 8). A striking difference appears in the change of slope of the Regordosa data for the not-inoculated irons when the CE equation included the effect of Mg (Figure 11b). The T_{LA} line changes slope and the data range from slightly hypo- to hyper-eutectic. Thus, if the effect of Mg is ignored, the irons appear to be hypoeutectic with a eutectic invariant of about 4.45% CE_{Eq} which changes to 4.40% when the influence of Mg on CE is included. This change also reflects the effects of holding in the furnace on the Si, on the residual Mg and on the nucleation potential. The iron is initially eutectic and the combined loss of Si (that moves C_{Eut} to the right) and Mg (that moves C_{Eut} to the left) keeps it eutectic.

Figure 11, and in particular the Regordosa data, clearly demonstrates the importance of including the effect of Mg in the calculation of CE. It further supports the contention that the eutectic composition can be determined from TA as the intersection between the T_{LG} and the T_{LA} liquidus lines, regardless of the equation for CE. However, the equation that accounts for the effect of Mg produces a lower CE and may shift the iron from hyper- to hypo-

eutectic. This has significant implications in the use of the effect of Mg on the analysis of TA data to understand the solidification of SG iron.

Selected data were also plotted on the Fe-C-2.5% Si isopleth (Fig. 12). As for the Chaudhari data, the Regordosa and Anjos data show that the convergence of the liquidus lines is to the right of the 3.7% eutectic carbon. This is in line with the previous conclusion that Mg additions move the eutectic invariant to higher carbon. The slopes of T_L for both data indicate that they are hypoeutectic, even though some of the data are to the right of the isopleth eutectic. It was also noted that significant eutectic undercooling and that the experimental SG iron eutectic is undercooled as much as 31 °C with respect to the equilibrium.

The T_{LA} Regordosa data that have a 2.4–2.5% Si range lie above the Chaudhari data by a significant 21 °C in average (Figure 12). This translates to a higher displacement to the right of the eutectic composition. The explanation resides in the different processing condition, and in particular in the fact that in the first case the Mg treatment was performed with Ni-Mg alloy, while in the second one with
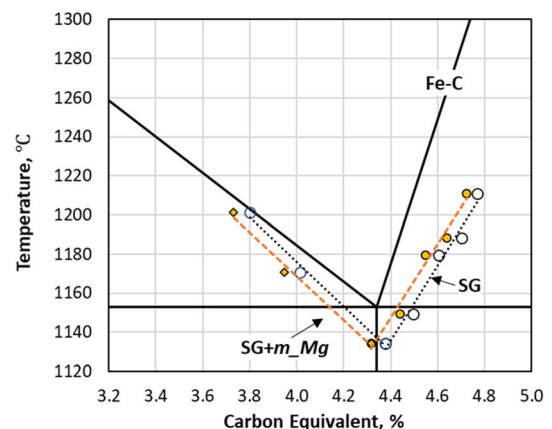

Figure 10. Austenite and graphite liquidus of uninoculated SG irons as a function of carbon equivalent superimposed on the Fe-C diagram; data with about 2.5% Si from ref. 4; calculations with the Thermo-Calc-based Eqn. 25 using $m_{Mg}=0$ for SG and $m_{Mg}^{exp}=-1.05$ for SG+m_Mg.
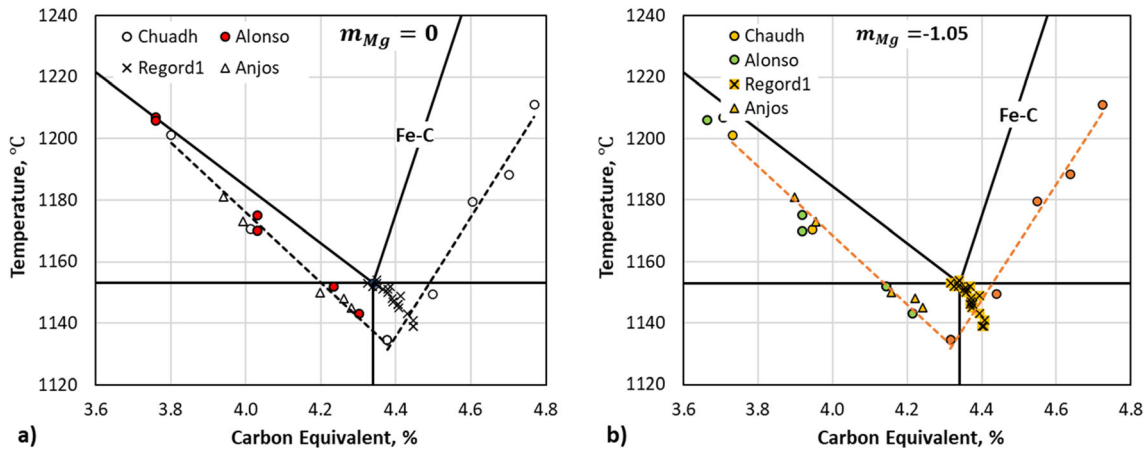
Figure 11. Experimental data on SG irons from various investigators; C_{Eq} calculated with Eqn. 21: (a) for $m_{Mg} = 0$; (b) for $m_{Mg}^{exp} = -1.05$; data source: Chaudh (average %Si of 2.5)—ref. 4, Alonso (average %Si of 1.7)—ref. 34, Anjos (average %Si of 2.1)—ref. 35, Regord1 (average %Si of 2.4)—ref. 36

Mg-FeSi alloy, which means that the two melts had different nucleation potentials. Thus, a closer analysis of the effect of inoculation is necessary.

A more detailed analysis of the effect of Mg on inoculated irons is given in Figure 13 that presents a comparison of data for Mg-treated irons when the CE was calculated with Eqn. 25, with and without the effect of Mg. Both data sets follow the same trend and are displaced to the left when Mg is included in calculation.

Effect of Inoculation

The effect of inoculation on 2.39–2.45% Si SG irons can be assessed form the analysis of the Regordosa holding experiments in Table 8. The liquidus temperature is plotted in Figure 14a as a function of the %Mg analyzed. The holding time runs in the opposite direction with the Mg content. It is seen that immediately after the Mg treatment when the Mg level is 0.043%, the $\Delta T_L = T_L^{inoc} - T_L^{noinoc}$ is of 8 °C. As the holding time increases, the Mg content and the nucleation potential decrease and ΔT_L decreases and mostly disappears at 0.02% Mg. This demonstrates convincingly the effect of Mg and/or inoculation on the measured liquidus arrest, and therefore on the estimation of the carbon equivalent through TA. Both the not-inoculated and inoculated data are slightly to the right of the Chaudhari data (Figure 14b) and mostly eutectic. The effect of inoculation is inconclusive, although a slight change in the slopes of the liquids lines is visible. Both lines have a trend typical for hypoeutectic irons.

Extensive research by Anjos [35] suggested that the solidification morphology of the melt for composition above the eutectic point is highly dependent on the inoculation
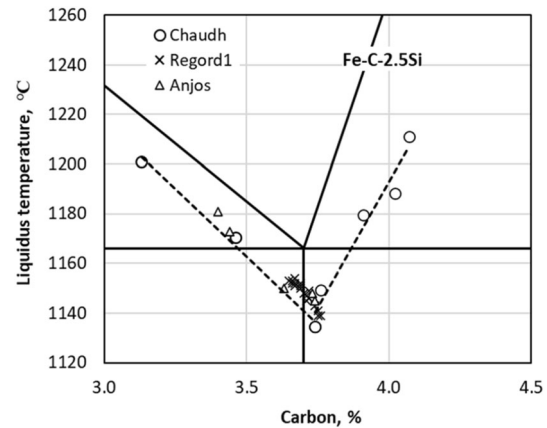

Figure 12. Experimental data for SG irons plotted as a function of carbon superimposed on the Fe-C.5Si isopleth. Data from Chaudhari (Table 5), Regordosa (Table 8), and Anjos (Table 7).

potential of the melt. If the melt has a low inoculation potential, it will still have hypoeutectic solidification morphology, although the CE is characteristic of eutectic and even hypereutectic composition. Such observations are supported by SinterCast that considers the inoculant to be the main determinator of the solidification mode [38]. This supports the contention that the use of the CE as a control parameter of the solidification morphology of the melt is not straightforward.

The effect of inoculation on the T_{LG} of high-Si (average 3.95% Si) SG irons can also be evaluated from the new data published by Regordosa et al. [10] summarized in Appendix (Table 9). These data were obtained from 1TC cups poured at increasing holding times from a pressure-pour furnace. They are presented in Figure 15. We first note that for both inoculated and non-inoculated Regordosa

data the *CE* slightly decreases in time, concomitantly with a significant decrease in the liquidus temperature (Figure 15a). This appears to be the effect of fading. In both cases, the slopes of the two lines imply that they belong to hypereutectic irons, which is confirmed on the data shown on the Fe-C-3.9% Si isopleth (Figure 15b). Therefore, all liquidus lines should be labeled as T_{LG}, and not as T_{LA}. Based on this, the concern expressed by Lekakh [11] regarding the switching from hypoeutectic to hypereutectic mode because of inoculation of the SG iron, stated by Regordosa et al. [10], appears to be justified, as the irons appear to be hypereutectic already.

As optimization of the production process for CG iron seeks to produce irons as close as possible to the eutectic in order to maximize graphite precipitation and minimize shrinkage [40] and, as small variations in the treatment process may lead to large deviations in the eutecticity of the iron, it is of utmost importance to use the concept of carbon equivalent correctly, as TA allows the recognition of unique melt characteristics in real time. New research by Ai et al. [37] involved cored wire treatment of a batch of iron to produce CG, followed by wire inoculation with increasing amounts of wire (0.10–0.45% ferrosilicon) in 1TC TA sand cups. The experimental data are summarized in Table 10, where we calculated the silicon content of each cup based on the inoculant wire additions. They concluded that inoculation in the cup can cause the solidification pattern of the melt to evolve from hypoeutectic to eutectic and even low hypereutectic at 0.45% inoculant addition (Figure 16). In this last case, the nodularity was increased significantly.

The Ai data have been analyzed as other data in this paper, by generating the *CE*–temperature and carbon–temperature graphs in Figure 17. For the data plotted without Mg correction, the experimental eutectic composition for 0.3%
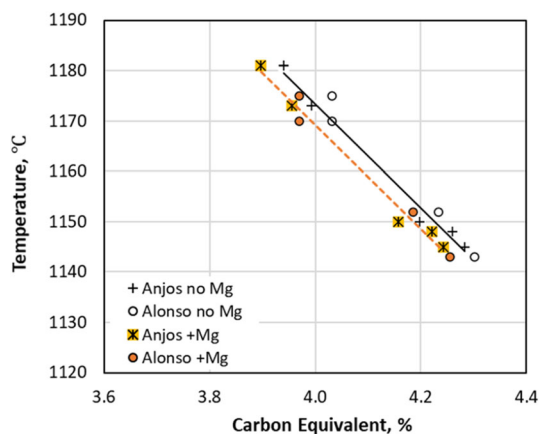

Figure 13. Experimental data of the austenite liquidus of inoculated SG irons from Alonso [34] and Anjos [35]; trendlines for Anjos data; black line and "no Mg"— calculations with Eqn. 25 $m_{Mg} = 0$. ; orange lines and "+Mg"—calculations with Eqn. 25 $m_{Mg}^{exp} = -1.05$.

inoculation appears to be at 4.22% *CE*, where the minimum of the liquidus temperature was recorded (Figure 17a). It is slightly lower than the Fe-C equilibrium C_{Eut} of 4.34. For the Mg-corrected data $C_{Eut} = 4.19$. In both cases the data sequence demonstrates that indeed inoculation can move a hypoeutectic iron to the hypereutectic region. This is, however, a combined effect of increased silicon and nucleation potential.

As the Si range in the data is from 2.14 to 2.39%, both the Fe-C-2%Si and Fe-C-2.5%Si isopleths were used. The Ai data are all hypoeutectic with respect to the Fe-C2Si isopleth, but slightly hypereutectic when compared to the Fe-C-2.5Si one. The isopleth diagram does not show the individual effect of silicon for the various inoculation levels.

The SinterCast Data

The previous analysis is based mostly on data obtained when using 1TC sand cups. Additional data on steel cups were provided by Dawson and Popelar [38]. The data were obtained from a stepping trial that consisted in increasing the Mg content to change the iron from CGI to ductile iron. The trials were done on 1-tonne ladles, using series production base iron. A low-sulfur ladle was tapped from a holding furnace. Then, additions of Mg and inoculant by cored wire were made, followed by obtaining the SinterCast TA cups after each step. The TA critical temperatures were extracted from the cooling curves, summarized in Table 11 and plotted in Figure 18. For comparison, data from Ai et al. [37] and Stefanescu et al. [24] on CG irons were also included. All SinterCast data are significantly hypoeutectic on the Fe-C diagram, corrected or uncorrected for Mg, and on the Fe-C2Si isopleth diagram. (The %Si range of the SinterCast data was 1.97 to 2.17.)

The Sintercast data for the A and C alloys and the Ai data lineup roughly on parallel lines to the Fe-C T_L lines, but at higher undercooling, explained by the different measuring system (steel cup) and the low levels of inoculation in the Sintercast data. They also show the effect of Mg in decreasing the liquidus temperature that is most clearly visible for the C series. This demonstrates the excellent capabilities of the SinterCast process in managing the graphite shape in CG irons through the control of the Mg level as predicted by their TA system. No significant changes are seen when the effect of Mg on *CE* was included (Figure 18c). It is interesting to note (Table 11) that the T_L plateau in SinterA remained constant despite four or five Mg addition steps, increasing the Mg from approximately 0.020 to 0.033%. In SinterC, the T_L plateau decreased linearly with each Mg-addition step, indicating that additional factors were involved in determining the T_L plateau in Melt C.
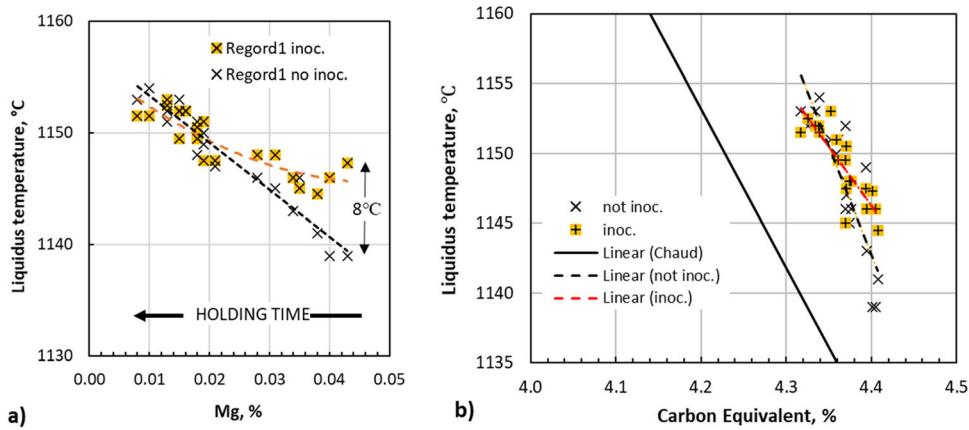
Figure 14. Effect of holding Mg-treated iron in the furnace on the experimental liquidus temperature of inoculated and non-inoculated SG irons: (a) effect of residual Mg; (b) correlation of liquidus temperature and the CE calculated with Eqn. 25 with $m_{Mg}^{exp} = -1.05$. Data from ref. 36.
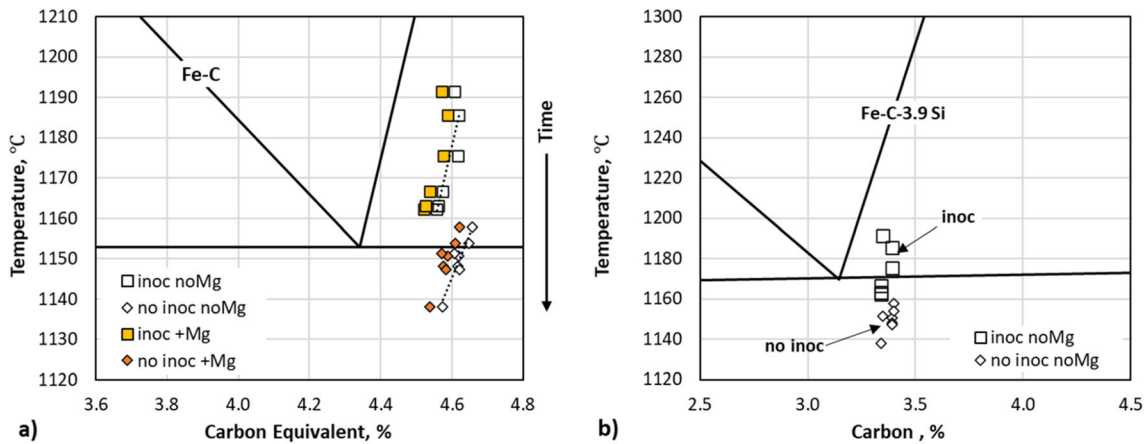

Figure 15. Analysis of experimental data on high-Si SG irons from Regordosa et al. [10] Table 9; (a) CE-liquidus data calculated with Eqn. 25, with $m_{Mg}^{exp} = -1.05$ (full squares) and with $m_{Mg}^{exp} = 0$ (empty squares); (b) data superimposed on the Fe-C-3.9% isopleth equilibrium phase diagram.
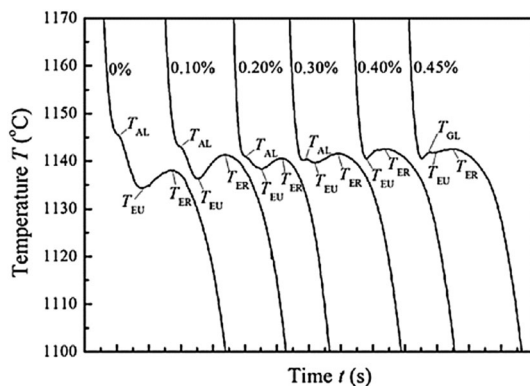

Figure 16. Effect of inoculation on the TA curves of CG irons [37].

Further analysis of the SinterCast data is provided in Figure 19. The two sets of data have very different behaviors. SinterC data show that both T_{LA} and $\Delta T = TE_{max} - TE_{min}$

decrease with higher magnesium. For SinterA, only the ΔT decreases.

A comparison between the Ai and SinterCast data is done in Figure 20. It is apparent that all liquidus lines are significantly undercooled with respect to the eutectic line. For the Ai 0.3% inc. line, the liquidus may be confused for a T_{EN} arrest. However, as the iron is still hypoeutectic, it is a T_{LA} arrest.

Effect of Melting Conditions

The melting process, which is quite different from foundry to foundry, has a significant effect on the chemical composition and nucleation potential of the melt, generally referred to as the melt quality. While a large number of the base and alloying elements in the melt are monitored by the foundry, others like trace elements and gasses are seldom part of the process control operations.
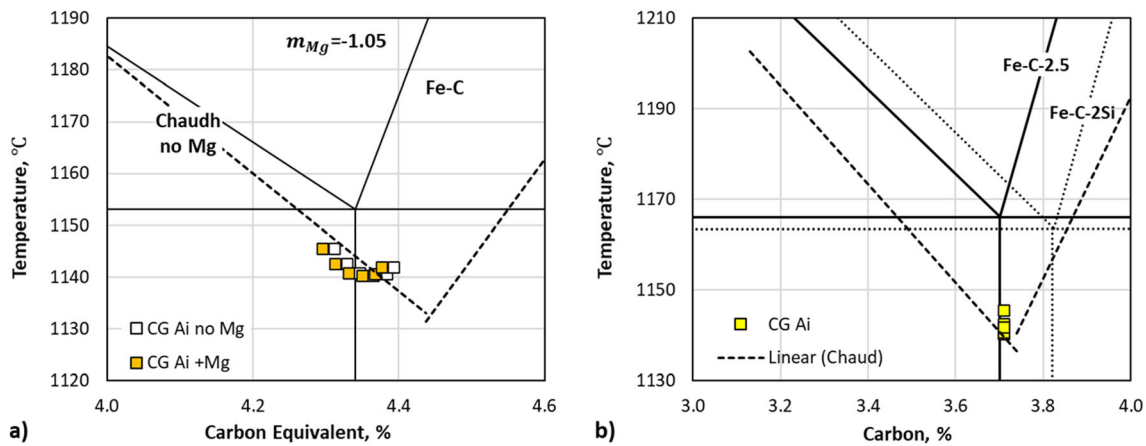
Figure 17. *Experimental data on SG and CG irons from various investigators superimposed on equilibrium phase diagrams: (a) on the Fe-C diagram; C_{Eq} calculated with Eqn. 25 ($m_{Mg} = 0$) for Chaudhari (dotted trend line) and Ai (symbol CG Ai no Mg); C_{Eq} calculated with Eqn. 25 ($m_{Mg}^{exp} = -1.05$) for Ai (symbol CG Ai + Mg); (b) on the Fe-C-2Si and Fe-C-2.5 isopleth; Chaudh—ref. 4, Ai—ref. 37.*

Early work by Heine and Henschel [41, 42] has demonstrated that the oxygen in the melt has a significant influence on the liquidus temperature. Regression analysis on experimental data obtained from iron melts produced under different conditions generated the following equations:

- For iron melted under argon (deoxidized):

$$T_{LA} = 1569 - 97.3 \cdot (\%C + 0.25 \cdot \%Si + 0.5 \cdot \%P) \ in \ °C$$
$$\text{Eqn. 26}$$

- For iron melted under oxidizing atmosphere:

$$T_{LA} = 1594.4 - 102.2$$
$$\cdot (\%C + 0.25 \cdot \%Si + 0.5 \cdot \%P) \ in \ °C \qquad \text{Eqn. 27}$$

To illustrate these effects, the two conditions are plotted in Figure 21a for Chaudhari et al. data. It is seen that melting under argon which results in a deoxidized melt decreases the T_{LA} as compared with the original Chaudhary data by an average of 4 °C, while oxidizing the melt increases it with the same amount on average. This is because deoxidation reduces the number of oxide inclusions that can act as nuclei, while oxidation increases it.

The effect of superheating can be estimated using the equation developed for iron melted after superheating over 1510 °C [41, 42]:

$$T_{LA} = 1550 - 92.06 \cdot (\%C + 0.25 \cdot \%Si + 0.5 \cdot \%P) \ in \ °C$$
$$\text{Eqn. 28}$$

As seen in Figure 21b, superheating produces an undercooling of the austenite liquidus with respect to the original Chaudhari data of 6 °C in average over the temperature interval considered. This undercooling is the result of the decreased nucleation potential because of coalescence and flotation of inclusions that can act as nuclei.

Eutectic Temperature

Early work by Basutkar et al. [16] quantified the effect of Si on the eutectic temperature of SG iron:

$$T_{EUT} = 1154.4 + 6.5 \cdot \%Si \qquad \text{Eqn. 29}$$

Later work [29] showed that the effect of alloying elements on the stable eutectic temperature of cast iron can be estimated through the equation:

$$T_{EUT} = 1154°C + 5.4 \cdot \%Si - 4.5 \cdot \%Mn + 6.4 \cdot \%Cu$$
$$- 18.7 \cdot \%P - 20 \cdot \%S$$
$$\text{Eqn. 30}$$

Note that both the Fe-C eutectic temperature and the coefficient for silicon in this equation (1154 °C and 5.4) are very close to Basutkar calculations (1154.4 °C and 6.5).

Multiple regression analysis on their trove of experimental data allowed Chaudhari et al. [43] to assess the effect of Mg on the eutectic temperatures in °C:

$$T_{EU} = 1960 + 23.4 \cdot (C + 0.68 \cdot \%Si - 1.73 \cdot \%Mg)$$
$$T_{ER} = 1978 + 19.8 \cdot (C + 0.84 \cdot \%Si - 2.9 \cdot \%Mg)$$
$$\text{Eqn. 31}$$

Conclusions

The answer to the question "can TA alone identify the eutectic invariant for a multicomponent Fe-C-Si alloy?", or, in other words "can the use of carbon equivalent equations allow establishing whether a multicomponent Fe-C alloy is eutectic or not?" is not a simple one. We have shown that if enough data are available to plot both the T_{LA} and T_{LG} lines, their intersection locates the experimental
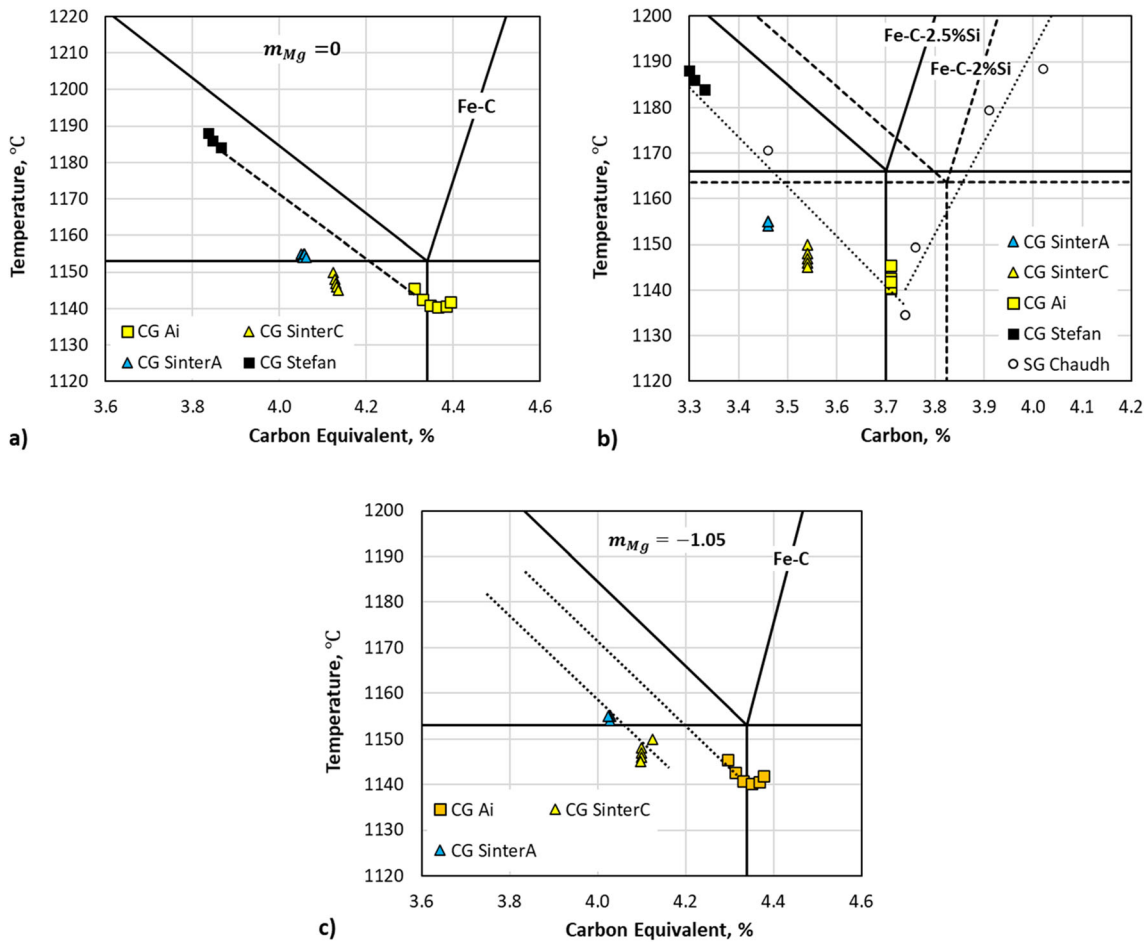
Figure 18. *Experimental data on SG and CG irons from various investigators: (a) superimposed on the Fe-C equilibrium phase diagram, C_{Eq} calculated with Eqn. 25 ($m_{Mg} = 0$); (b) superimposed on Fe-C-Si isopleths; (c) superimposed on the Fe-C phase diagram, C_{Eq} calculated with Eqn. 25 ($m_{Mg} = -1.05$); Chaud—ref. 4, Stefan—ref. 24, Ai—ref. 37, Sinter—ref. 38; full lines—the binary Fe-C diagram; dotted lines—regression lines for Chaudhari data.*
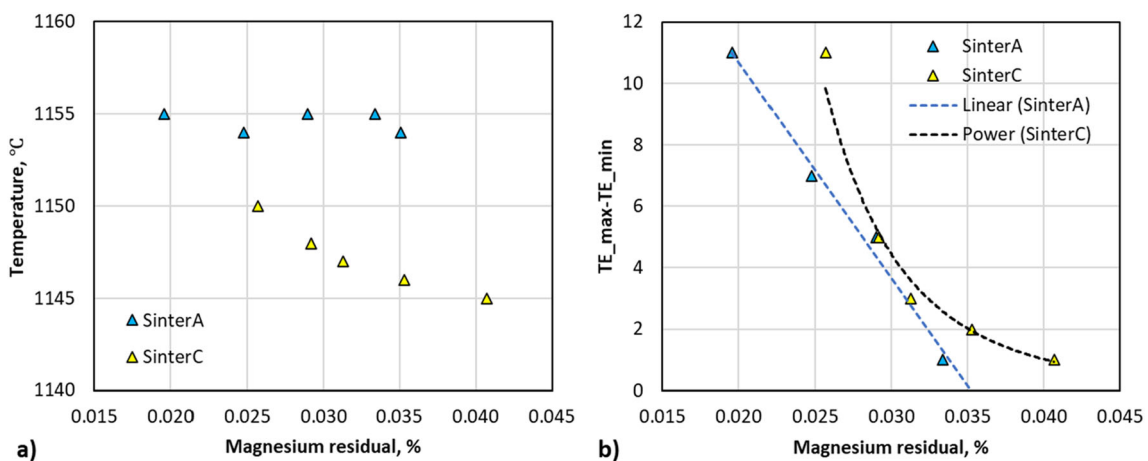
Figure 19. *Correlation between some critical temperatures and magnesium residual: (a) liquidus temperature; (b) $\Delta T = TE_{max} - TE_{min}$.*

eutectic carbon. This is reliable information, regardless of the equation used for *CE*. Unfortunately, this information is not readily available in industrial applications that are typically limited to a narrow compositional range. This begs the question: is the *CE* a sufficiently accurate number in defining the chemistry of the metal? The answer is

Figure 20. Comparison of Ai et al. [37] and SinterCast series C [38] data; the curves are displaced in time to facilitate interpretation.

ambivalent, as discussed throughout the paper: no, when determined from the liquidus of TA curves, because it is affected by both processing and measuring system variables; yes, when it is calculated solely based on composition. In the first case we defined it as the kinetic CE, CE_{Kin}. In th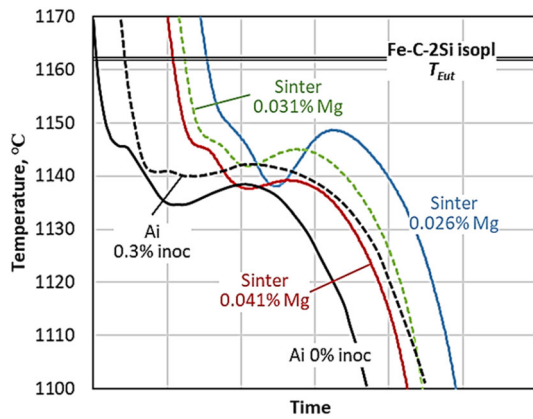e second case as the equilibrium CE, CE_{Eq}. Yet, even for CE_{Eq} the currently available equations are unsatisfactory for several reasons. The analysis in this paper demonstrates that the Mg content affects the eutectic invariant. This is also true for the oxygen content. As the solubility factors of these elements are not readily available, there are no thermodynamics calculations that include these elements in the CE_{Eq} equation. It was also demonstrated that Mg treatment moves the liquidus temperature lines and the eutectic carbon to the left on the carbon equivalent temperature graph. It decreases both the liquidus temperature and the eutectic temperature and increases the

eutectic carbon. The solubility factor of Mg, m_{Mg}, was evaluated from experiments to be about −1.05. This number lies between the experimental −0.7 calculated by Basutkar et al.[16] and the thermodynamic guess of −6 proposed by Yamane et al.[5]. Yet, more work should be done on this subject, as m_{Mg}^{exp} appears to be dependent on temperature. Furthermore, the assumption that m_{Si} is a unique number independent of the Si content was demonstrated to be inaccurate. A new equation for CE_{Eq} that includes the effect of Mg and of Si was offered. It helps decide whether a liquidus arrest close to the eutectic is an austenite or graphite liquidus.

Experiments by Ai et al. [37] have demonstrated that under certain circumstances, inoculation moves the eutecticity of the iron to the right, from hypo-eutectic toward hyper-eutectic, a combined effect of the increase in the nucleation potential and of silicon.

The foundries are using CE_{Kin} for composition control through the $CE_{Kin} - T_L$ correlation. Yet, as shown throughout the paper, this correlation is affected by the holding time in the furnace, which changes the metal quality (nucleation potential, oxygen level) even when the major elements are not significantly altered, as well as by inoculation. In this work, it was found that inoculation may increase T_L by as much as 8°C.

Although CE as determined by TA is not an exactly defined number, it is still a reliable tool for the control of metal quality. It is reproducible, but it is foundry specific. A unique CE equation cannot be used as a measure of eutecticity by all foundries, as it is process-specific. The input of the foundry metallurgist in adjusting the CE_{Kin} to the particularities of that foundry process is vital.
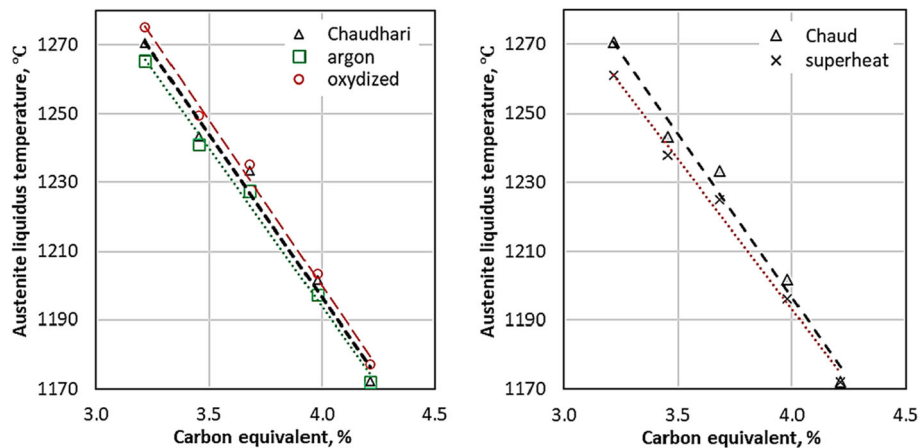

Figure 21. Effect of melting conditions on the austenite liquidus temperature on LG iron: (a) effect of the degree of oxidation of the melt; (b) effect of melt superheating; CE_{Eq} (Eqn. 13).

Acknowledgements

Appendix—Data base

See Tables 5, 6, 7, 8, 9, 10 and 11.

Table 5. Data Compiled from the Graphs in Chaudhari et al. [4]; Ni-Mg Alloy Treatment; No Inoculation

SG irons						Base irons			
Alloy	%C	%Si	%Mg	T_L °C	T_{EN} °C	Alloy	%C	%Si	T_L °C
1211	3.13	2.53	0.067	1201	–	1101	2.8	2.84	1233
3203	3.46	2.17	0.062	1171	–	1203	3.16	2.64	1202
1309	3.74	2.43	0.058	1134	1134	3201	3.53	2.2	1172
2203	3.76	2.72	0.056	1149	1142	1301	3.74	2.46	–
2303	3.91	2.6	0.055	1179	1146	2201	3.84	2.63	1204
1409	4.02	2.56	0.060	1188	1141	1401	4.06	2.56	1259
2407	4.07	2.61	0.042	1211	1154	2402	4.11	2.54	1279

Table 6. Data from Alonso et al. [34]; sandwich Mg-FeSi Treatment, in-Mold Inoculation

Alloy	Cool rate*	%C	%Si	%Mn	%P	%S	%Mg	T_L °C
110313	2.54	3.24	1.58	0.2	0.01	0.013	–	1228
80513	1.35	3.35	1.7	0.18	0.018	0.011	–	1220
150513	1.32	3.52	1.94	0.17	0.014	0.008	–	1189
150513	3.17	3.52	1.94	0.17	0.014	0.008	–	1179
220513	4.11	3.55	2.02	0.18	0.017	0.008	–	1161
60613	Top	3.80	1.78	0.21	0.013	0.006	0.046	1152
110313	5.21	3.35	1.70	0.21	0.009	0.011	0.050	1207
90713	3.41	3.65	1.60	0.17	0.011	0.006	0.058	1175
110313	6.90	3.35	1.70	0.21	0.009	0.011	0.050	1206
90713	4.41	3.65	1.60	0.17	0.011	0.006	0.058	1170
160513	3.34	3.86	1.81	0.20	0.011	0.005	0.045	1143

*in °C/s at ~1272 °C

Table 7. Data from Anjos [35]; Mg-FeSi Treatment, Inoculation in Cup

%C	%Si	%Mn	%P	%S	%Mg	T_L °C
3.40	2.11	0.24	0.026	0.007	0.041	1181
3.44	2.15	0.234	0.025	0.007	0.035	1173
3.63	2.20	0.271	0.028	0.006	0.039	1150
3.73	2.08	0.28	0.028	0.007	0.037	1148
3.74	2.12	0.268	0.026	0.007	0.038	1145

Table 8. Data Compiled from Regordosa et al. [36] Figure 9; Mg-FeSi Treatment

Alloy	%C	%Si	%Mn	%P	%Cu	%Mg	T_L °C *not inoc*	T_L °C*inoc.*
A	3.75	2.45	0.64	0.022	0.85	0.043	1139	1147
B	3.76	2.42	0.63	0.023	0.85	0.040	1139	1146
C	3.75	2.45	0.63	0.024	0.85	0.038	1141	1145
D	3.74	2.43	0.64	0.022	0.85	0.034	1143	1146
E	3.72	2.42	0.63	0.023	0.84	0.035	1146	1145
F	3.71	2.45	0.63	0.025	0.84	0.031	1145	1148
G	3.72	2.42	0.63	0.022	0.84	0.028	1146	1148
H	3.71	2.41	0.64	0.022	0.84	0.021	1147	1148
I	3.72	2.44	0.63	0.024	0.84	0.019	1149	1148
J	3.69	2.43	0.64	0.023	0.83	0.019	1150	1151
K	3.70	2.43	0.62	0.025	0.83	0.018	1148	1151
L	3.69	2.43	0.64	0.026	0.83	0.018	1151	1150
M	3.67	2.42	0.63	0.021	0.83	0.016	1152	1152
N	3.69	2.45	0.63	0.022	0.83	0.015	1152	1150
O	3.66	2.43	0.63	0.025	0.83	0.015	1153	1152
P	3.67	2.45	0.62	0.025	0.82	0.013	1151	1153
Q	3.66	2.40	0.62	0.023	0.83	0.013	1152	1153
R	3.67	2.40	0.62	0.023	0.83	0.010	1154	1152
S	3.65	2.39	0.62	0.022	0.83	0.008	1153	1152

Table 9. Data from Regordosa et al. [10]; Composition is for the Non-Inoculated iron; T_{LA} and T_{LG} Notations as per ref. [10]

Alloy	%C	%Si	%Mn	%Mg	T_{LA} °C*non-inoc.*	T_{LG} °C*inoc.*
942	3.39	3.95	0.20	0.031	1151	1186
952	3.35	4.01	0.20	0.034	1151	1192
1005	3.40	4.01	0.20	0.034	1158	–
1015	3.40	3.99	0.20	0.036	1154	–
1025	3.39	3.94	0.20	0.038	1148	1176
1040	3.39	3.95	0.19	0.036	1147	–
1142	3.34	3.92	0.20	0.034	–	1162
1149	3.34	3.93	0.20	0.033	–	1163
1205	3.34	3.96	0.19	0.035	1138	1167

Table 10. Data from Ai et al. [37] for Wire-Inoculated CG irons

Inoc %	%C	%Si	%P	%S	%Mn	%Cu	%Mg	T_L °C	T_{EU} °C
0	3.71	2.14	0.024	0.01	0.314	0.69	0.015	1146	1134
0.10		2.20						1143	1136
0.20		2.25						1141	1138
0.30		2.31						1140	1140
0.40		2.36						1141	1141
0.45		2.39						1142	1142

Note The C, P, S, Mn, Cu and Mg content are assumed to be the same for all TA cups.

Table 11. Data from Dawson and Popelar [38]; CR is the Cooling Rate in °C/s

Alloy	inoc	%C	%Si	%Mn	%P	%S	%Mg	T_L	TE_{min}	TE_{max}	CR
A base	–	3.46	1.97	0.393	0.01	0.0040					
A1	0		1.97				0.020	1155	1139	1150	2.20
A2	1		1.98				0.025	1154	1141	1148	1.32
A3	2		1.99				0.029	1155	1140	1145	1.75
A4	3		2.00				0.033	1155	1141	1142	1.42
A5	4		2.00				0.035	1154	1136	1137	
C base	–	3.54	1.95	0.419	0.01	0.0028					
C1	0		1.95				0.026	1150	1138	1149	2.15
C2	1		1.96				0.029	1148	1142	1147	2.17
C3	2		1.97				0.031	1147	1142	1145	2.20
C4	3		1.98				0.035	1146	1139	1141	1.82
C5	4		1.98				0.041	1145	1138	1139	1.60

Note inoculation is given in m of inoculant wire added in the ladle.

REFERENCES

1. D.M. Stefanescu, R. Suarez, S.B. Kim, 90 years of thermal analysis as a control tool in the melting of cast iron. China Found. **17**(2), 69–84 (2020)
2. H. Okamoto, The C-Fe (Carbon-Iron) system. J. Phase Equilibria **13**(5), 543–564 (1992)
3. Neumann, F. The Influence of Additional Elements on the Physico-Chemical Behavior of Carbon in Carbon Saturated Molten Iron, in: Recent Research on Cast Iron, H.D. Merchant, Ed., Gordon and Breach, 1968, p 659
4. M.D. Chaudhari, R.W. Heine, C.R. Loper, Principles involved in the use of cooling curves in ductile iron process control. AFS Trans. **82**, 431–440 (1974)
5. K. Yamane, H. Yasuda, A. Sugiyama et al., Influence of Mg on solidification of hypereutectic cast iron: x-ray radiography study. Metall. Mater. Trans. A **46A**, 4937–4946 (2015)
6. R.E. Boeri, M.G. López, N.E. Tenaglia, J.M. Massone, Solidification, macrostructure and shrinkage formation of ductile and compacted irons. Inter Metalcast **14**, 1172–1182 (2020). https://doi.org/10.1007/s40962-020-00444-z
7. S. Engler, R. Ellerbrok, On the growth of an austenite shell on the graphite nodule during the solidification of iron-carbon-silicon melts. Giesserei-Forschung **4**, 141–145 (1977)
8. D.M. Stefanescu, Microstructure evolution during the liquid/solid transformation in cast iron, in *ASM handbook cast iron science and technology*, vol. 1A, ed. by D.M. Stefanescu (ASM International, Materials Park Ohio, 2017), pp. 59–80
9. H.L. Zhao, M.F. Zhu, D.M. Stefanescu, Modeling of the divorced eutectic Sslidification of spheroidal graphite Ccst iron. Key Eng. Mater. **457**, 324–329 (2011). https://doi.org/10.4028/www.scientific.net/KEM.457.324
10. A. Regordosa, J. Sertucha, J.R. Olaizola et al., When is a cast iron eutectic? Inter Metalcast (2021). https://doi.org/10.1007/s40962-021-00587-7
11. S.N. Lekakh, Technical Discussion Appendix, Comments on A. Regordosa, J. Sertucha, J. Ramón Olaizola, J. Lacaze article "When is a cast iron

eutectic?" Inter Metalcast (2021). https://doi.org/10.1007/s40962-021-00587-7

12. Ledebur, A. Handbuch der Eisen und Stahl Giesserei, Weimar, 1982, p 342

13. E. Piwowarsky, *Hochwertiges Gusseisen* (Springer, Heidelberg, 1942)

14. M. Schwarz, A. Vath, Giesserei **20**, 373 (1933)

15. C.R. Loper, R.W. Heine, W. Reesman, B.H. Shah, Thermal analysis of ductile iron. AFS Trans. **89**, 541–547 (1967)

16. P.K. Basutkar, R.W. Heine, C.R. Loper, Effect of magnesium and cerium additions on the Fe-C-Si diagram. AFS Trans. **81**, 336–340 (1973)

17. U. Kuehn, An old process and a new measurement technology: thermal analysis. Cast. Online Mag. **11**, 18–24 (2020)

18. D.A. Sparkman, Microstructure by thermal analysis. AFS Trans. **119**, 413–420 (2011)

19. U. Kuehn, Probengefaess zur Analyse von Schmelzen. German Patent **10209427**, 2 (2005)

20. V. Anjos, R. Deike, C. Silva Ribeiro, The use of thermal analysis to predict the dendritic coherency point on nodular cast iron melts. Ciência & Tecnologia dos Materiais **29**, 27–33 (2017)

21. Dawson, S., Popelar, P. Thermal analysis and process control for compacted graphite iron and ductile iron. SinterCast (2014) www.sintercast.com

22. E.F. Ryntz, J.F. Janowak, A.W. Hochstein, C.A. Wargel, Prediction of nodular iron microstructure using thermal analysis. AFS Trans. **79**, 141–144 (1971)

23. L. Bäckerud, K. Nilsson, H. Steen, Study of nucleation and growth of graphite in magnesium treated cast iron by means of thermal analysis, in *The metallurgy of cast iron*. ed. by B. Lux, I. Minkoff, F. Mollard (Georgi Publishing Co., Switzerland, 1975), pp. 625–636

24. D.M. Stefanescu, F. Martinez, I.G. Chen, Solidification behavior of hypoeutectic and eutectic compacted graphite cast irons. chilling tendency and eutectic cells. AFS Trans. **91**, 205–216 (1983)

25. Kuehn, U. Private communication, 2021

26. J.G. Humphreys, BCIRA J. **9**, 609–621 (1961)

27. Heine, R.W. The carbon equivalent Fe-C-Si diagram and its application to cast irons. AFS Cast Metals Res. J. 49–54 (1971)

28. R. Sillén, Finding the true eutectic point – an essential task for efficient process control of Ductile Iron. Ductile Iron News **2**, 100–104 (2007)

29. D.M. Stefanescu, J. Lacaze, Thermodynamics Principles as Applied to Cast Iron, in ASM Handbook, Vol. 1A, *Cast iron science and technology*, ed. by D.M. Stefanescu (ASM International, Materials Park, OH, 2017), pp. 31–45

30. R.C. Creese, G.W. Healy, Metallurgical thermodynamics and the carbon equivalent equation. Met. Trans. B **16B**, 169 (1985)

31. R.W. Heine, The Fe-C-Si solidification diagram for cast irons. AFS Trans. **94**, 391 (1986)

32. V.E. Bazhenov, M.V. Pikunov, Determining the carbon equivalent of cast iiron by the thermo-calc program. Steel Trans. **41**(11), 896–899 (2011). https://doi.org/10.3103/S0967091211110027

33. M. Castro, M. Herrera, M.M. Cisneros et al., Simulation on thermal analysis applied to the description of the solidification of hypereutectic SG irons. Int. J. Cast. Metals Res. **11**, 369–373 (1999)

34. G. Alonso, D.M. Stefanescu, R. Suárez et al., Kinetics of graphite expansion during the solidification of lamellar and spheroidal graphite iron. AFS Trans. **122**, 237–248 (2014)

35. Anjos, V. Use of thermal analysis to control the solidification morphology of nodular cast irons and reduce feeding needs. Doktors der Ingenieurwissenschaften Dr.-Ing. genehmigte Dissertation, University of Duisburg-Essen, 22 July 2015

36. A. Regordosa, U. de la Torre, J. Sertucha, J. Lacaze, Quantitative analysis of the effect of inoculation and magnesium content on compact graphite irons — experimental approach. J. Mater. Res. Technol. **9**(5), 11332–11343 (2020)

37. S. Ai, Z. Xu, Z. Liu et al., Evolution of inoculation thermal analysis and solidification morphology of compacted graphite iron. Kovove Mater. **59**, 51–57 (2021). https://doi.org/10.4149/km2021151

38. S. Dawson, P. Popelar, SinterCast, Katrineholm, Sweden, private communication, 2021

39. E.N. Pan, K. Ogi, C.R. Loper, Analysis of the solidification process of compacted/vermicular graphite cast iron. AFS Trans. **90**, 509–527 (1982)

40. A.K. Ramos, A. Diószegi, W.L. Guesser, C.S. Cabezas, Microstructure of compacted graphite iron near critical shrinkage areas in cylinder blocks. Inter Metalcast **14**, 736–744 (2020). https://doi.org/10.1007/s40962-019-00403-3

41. R.W. Heine, Liquidus and eutectic temperatures and solidification of white cast irons. AFS Trans. **85**, 537–543 (1977)

42. C. Henschel, R.W. Heine, Some effects of oxygen on solidification of cast iron. AFS Cast Metals Res J Sept. **2**, 93–104 (1977)

43. C.R. Loper, R.W. Heine, M.D. Chaudhari, Thermal analysis for structure control, in *The metallurgy of cast iron*. ed. by B. Lux, I. Minkoff, F. Mollard (Georgi Publishing Co., St Saphorin, Switzerland, 1975), pp. 639–657